Canopy Characterization of Sweet Chestnut Coppice in the North of Spain From Lidar Data

Marta Prada (mprada@cetemas.es)
CETEMAS
Elena Canga
CETEMAS
Juan MAJADA
CETEMAS
Celia Martínez-Alonso
CETEMAS

Research

Keywords: Canopy vertical profile, Castanea sativa Mill., Map tool, LAIe model, Canopy layers

Posted Date: February 10th, 2021

DOI: https://doi.org/10.21203/rs.3.rs-172988/v1

Version of Record: A version of this preprint was published at European Journal of Forest Research on January 29th, 2022. See the published version at https://doi.org/10.1007/s10342-021-01436-2.

Abstract

One important part of a forest stand that is impacted by forest management is the canopy structure. Canopy structure is closely related to ecosystem functions as it plays an important role in the relationships between structural complexity, biodiversity and stand productivity. The Leaf Area Index (*LAI*) is a key parameter that helps to understand the connection between canopy structure and ecosystem functions. In this study, the main aims were to examine the impact of forest management on canopy structure using LiDAR data to characterize the canopy vertical profile, the development of *LAI* models and a descriptive mapping tool for sweet chestnut (*Castanea Sativa* Mill.) coppice. Twenty-one circular plots (r=10m) were established, each of which was submitted to one of the following forest management treatments: Control, with no intervention (3300-3700 stems ha^{-1}); Treatment 1, one thinning to leave a living stock density of 900–600 stems ha^{-1}; or Treatment 2, a more intensive thinning, leaving 400 stems ha^{-1}. An *LAI* field measurement was made in all plots and the study area was recorded by LiDAR. With the LiDAR two types of metrics were calculated: standard elevation metrics and canopy metrics. The latter allowed the complete characterization of the canopy from ground to maximum height. The results showed the different canopy layers of the study area, highlighting how the resprout layer influences the canopy structure of sweet chestnut coppice. By combining the LiDAR data and the *LAI* field estimates various linear and non-linear models were developed and tested, the linear model being found to have the best accuracy for the study area (Cross-validation: R^2 (0.79) and *RMSE* (0.20)). With the selected linear model and other LiDAR data of interest such as the 95^{th} percentile, an automatic mapping tool was designed. This tool allows spatially information to be generated that can be used to implement management strategies to improve productivity, ecosystem functions, forest management planning and/or fuel management.

Introduction

Forests are highly complex systems influenced by numerous external and internal factors, making the development of sustainable forest management strategies, though crucial, somewhat challenging (Ceccherini et al., 2020).

Forest management operations impact on the complete forest ecosystem. For example, thinnings not only result in increased diameter growth, but also provoke changes in canopy structure. Canopy structure refers to the organization, both horizontal and vertical, of the aboveground elements of vegetation including position, type, connectivity and quantity, as well as organization changes over time (Parker, 1995; Bréda, 2008). As such, it is closely related to ecosystem functions, playing an important role in the relationships between structural complexity, biodiversity, stand productivity, carbon balance and ecosystem services.

Estimates of canopy structure can be derived through the active remote sensing technology LiDAR (Light Detection and Ranging), which is able to directly characterize vertical forest structure (Coops et al., 2007; Lim et al., 2003; Lovell et al., 2003). LiDAR is an active sensor that uses light in the form of a pulsed laser

to measure the distance (as a function of time) between light being emitted from the sensor and that being reflected back off the target, thereby generating a 3D structure of the targeted element. As such, in a forest, the laser pulses from the LiDAR are not only reflected back from the canopy, but also from the ground and other vegetation elements in those places where the laser pulse travels through the gaps that exists in the canopy. This ability of LiDAR allows information to be retrieved about the underlying terrain, enabling better characterization of the different canopy layers (Nelson et al., 1988; Lesfky et al., 2002; Mkaouar et al., 2018). For these reasons, LiDAR technology has been investigated in depth in terms of its value in the acquisition of data related to forest biomass, wood volume, stem density, canopy height, canopy cover and forest inventory parameters and structural characteristics, among other applications (e.g. Popescu et al., 2002; Coops et al., 2007; Bergen et al., 2009; Leeuwen and Nieuwenhuis, 2010; Magnussen et al., 2018).

There is an important parameter that helps to understand the connection between canopy structure and ecosystem functions (Bréda, 2008), the Leaf Area Index (*LAI*). *LAI*, first described by Chen and Black (1992), “quantifies the total one-sided green leaf area per unit of ground surface as a dimensionless quantity”. In fact, *LAI* is used as a proxy of plant growth (Mkaour et al., 2018) and is considered a standard quantitative tool to quantify canopy through the assessment of foliage levels and leaf surface area (Bréda, 2008). As a result, *LAI* field measurement methods have been investigated in depth, where optical methods are those most commonly implemented in field measurements, such as the Canopy Light Analyzer LAI-2000/2200/2200C or hemispherical cameras (Jonckheere et al., 2004; Weiss et al., 2014). However, these methods are costly and time-consuming, hence there is need to develop another technique to evaluate *LAI.* In recent decades, therefore, considerable effort has been dedicated to estimating *LAI* from LiDAR data in vegetation environments with a variety of species and in different regions (e.g. Lovell et al., 2003; Jensen et al., 2008; Solberg et al., 2006, 2009, 2010; Richardson et al., 2009; Zhao and Popescu, 2009; Korhonen et al., 2011; Heiskanen et al., 2015; Pearse et al., 2017; Zhang et al., 2017; Qu et al., 2020). Some of these studies estimated *LAI* from the canopy gap fraction using the Beer-Lambert law and based on LiDAR data, and validated the models using *LAI* field estimates obtained with the optical instruments (Richardson et al., 2009; Solberg et al., 2009; Zhao and Popescu, 2009).

Since there is a clear relationship between canopy structure and *LAI* (Bréda, 2008), in 1999, Lefsky et al. adapted the use of LiDAR data to obtain the Canopy Vertical Profile (CVP), that is, the vertical distribution of the elements of the canopy from the ground to the maximum height. They also studied CVP according to different stand ages, from very young to old growth. This methodology was also employed in 2003 by Lovell et al. to obtain certain structural parameters such as cover, height and foliage profile. In 2007, Coops et al., used this same methodology to obtain CVPs, and also used a probability function to summarize and retrieve the CVP. Nowadays, these studies constitute the basis for the characterization of the differentiation of the canopy layer throughout CVP. However, it should be taken into account that LiDAR collects data on all forest canopy layers, including the understory, and in recent years LiDAR data have been employed not only to ascertain *LAI* associated with trees, but also that relating to understory components (Hamraz et al., 2017; Zhang et al., 2017; Mkaouar et al., 2018; Melo et al., 2019). This is

particularly interesting with respect to those species that resprout from a stump following felling as the regrowth generates an important additional layer in the understorey.

One such species is the sweet chestnut (*Castanea Sativa* Mill.), which is extensive across northwest of Spain, and is of great importance as it produces quality wood in relatively short rotations, mainly in coppiced form (Menéndez-Miguélez et al., 2014). This reality has provoked a growing interest from forest managers, owners and other stakeholders for new sustainable forest management tools for use with sweet chestnut. However, most traditional coppice stands have been abandoned or their rotation time has been increased considerably due to the socioeconomic changes that occurred in the past in rural areas (Conedera et al., 2004; Menéndez-Miguélez et al., 2013). Traditionally, silvicultural treatments such as thinning are not employed in the management of sweet chestnut coppice stands, meaning that the full potential of the species, which requires management in order to achieve quality timber, is not exploited (Mannetti et al., 2020). In this respect, in order to manage sweet chestnut for 'quality' wood production, further studies that consider and emphasize these aspects are needed, some of which are currently being developed (Prada et al. 2020).

In this context, the main aim of this study is to use LiDAR data to examine the impact of forest management on sweet chestnut coppice canopy structure through (1) the characterization of the vertical canopy structure from the ground to maximum height, (2) the development of *LAI* models and (3) the generation of a tool to estimate *LAI* and other variables for forest management planning at the large scale.

Materials And Methods

2.1. Study area

The research site is located in Redes Natural Park which occupies the eastern central area of the Principality of Asturias in the north of Spain (Figure 1). The annual rainfall ranges from 987 to 1351 mm, with an average annual temperature in the area of 10–11°C. The study site has a northern orientation with high slope (45-57%) and is between 600 and 700 metres above sea level. This study was conducted as a pilot forest management trial made up of three different treatments in sweet chestnut coppice stands: (1) Control, where there were no management operations (3300-3700 stems ha^{-1}), (2) Treatment 1, which consisted of one thinning that left a living stock density of between 600 and 900 stems ha^{-1} and (3) Treatment 2, which involved a more intensive thinning that resulted in a living stock density of around 400 stems ha^{-1}. Thinning treatments were carried out at the end of 2015, in winter when the sweet chestnut loses its leaves. In the Control and Treatment 1 plots Oak (*Quercus Petrea*) is also present.

2.2. Field data: Forest inventory and LAI measurements

Forest inventory data were collected from three established permanent plots (r=15 m) in the study area. Each tree in every plot was labelled and diameter (in cm) at breast height (*d*) (diameter at 1.3 m above the top of the stool) was measured with a tree calliper to the nearest 0.1 cm, as was total height (*h*), to the

nearest 0.1 m, using a digital hypsometer. Using this information certain stand variables were calculated to characterize the study area. These plots were inventoried twice: first in winter 2015 (installation year) and then in summer 2019 (Figure 2).

LAI field measurements were collected in July 2019, using an LAI-2200C plant canopy analyzer, from 21 circular plots (r=10 m). The location of the plots was based on a grid system whereby where each plot centre was separated from those around it by 30 m. The locations of the plot centres were recorded using a GPS TrimbleExplorer XH™ (Trimble, Sunnyvale, CA, USA) with submetric accuracy and the total number of *LAI* plots per trial depended on the total surface area covered by each treatment.

The LAI-2200C is a portable instrument, in this case consisting of a control unit and an optical sensor, that directly provides an *LAI* value that may include vegetation which is not leaves and is thus referred to as Effective *LAI* (henceforth here, LAI_e) (Chen and Black, 1992). This device has been widely used in LAI_e studies and several extensive review papers have established it as an appropriate tool for LAI_e field measurements (e.g. Bréda, 2008; Jonckheere et al., 2004; Morsdorf et al., 2006; Jensen et al., 2008; Solberg et al., 2009; Korhonen et al., 2011; Pearse et al., 2017; Fang et al., 2019). The LAI-2200C incorporates five concentric rings with central zenith angles of 7, 23, 38, 53 and 68 degrees in a “fish-eye” optical sensor, measuring in the blue band (320–490 nm). The measurements of LAI_e were made below the canopy and also in a clearing, the latter to simulate the light falling directly on the crown. These two measurements were required in order to calculate the ratio between the two transmittances (above and below the canopy). This ratio was recalculated into LAI_e as described in the instrument manual (LI-COR Inc., 2015). All measurements were performed under uniform overcast skies to reduce the effect of scattered light in the canopy and the sensor was equipped with a 90° view restrictor in accordance with the manufacturer’s instructions.

In the forest, LAI_e field measurements were conducted using the plot layout employed in similar previous studies (Solberg et al., 2006, 2009) within the circular plots mentioned above. In each plot, one measurement was taken at the plot centre, and another four—one at each cardinal point—were made at 3 metres from the centre. Due to the differences in the canopy cover, to guarantee a low standard error of LAI_e, supplementary measurements (n=18) were collected at random within the plot.

2.3. LiDAR data

LiDAR data were collected in leaf-on conditions in summer 2019, at the same time as the LAI_e field data were measured, using a Velodyne VLP-16 LiDAR scanner mounted on an unmanned aerial vehicle (drone). The laser wavelength of the device was 905 nm with a field of range of ±15˚ Vertical FOV / 360˚ Horizontal FOV. The sensor recorded a maximum of 2 returns per pulse, and a minimum density of 25 points m^{-2} was achieved over the area. LiDAR data was recorded for the all the stands in the study area, which included all the LAI_e plots.

To calculate the plot-level forest structural parameters, the following steps were followed in order to obtain the LiDAR metrics needed to model LAI_e for sweet chestnut coppice (Figure 3).

The LiDAR point cloud was classified as either background or not background with FUSION software V4.00 (McGaughey, 2020), after which the point cloud was normalized against the ground surface height. The LiDAR standard elevation metrics were also computed with FUSION taking different fixed radii starting with the 10 m radius established for the LAI_e plots in the field and increasing the radius by 2 m each time up to a limit of 30 m, following the methodology described by Pearse et al. (2017). This was done because the LiDAR and the LAI-2200c were not sampling the same canopy volume, LiDAR uses a vertical cylinder and the LAI-2220c an inverted cone. Moreover, since sweet chestnut resprouts from stump and this generates another canopy layer in addition to the principal one and because the volume of the cone depends on the height of the canopy, the LiDAR metrics were computed for different heights (2, 3, 4, 5 m). The optimum choice of the height threshold is crucial in this type of study in order to reliably identify ground hits as those that are below the height threshold and those above it as corresponding to the canopy (Zhao and Popescu, 2009). Following the testing of the various radii and height measurements, those most representative of the field measurements were selected to form the basis of the LiDAR standard elevation metrics.

Among the LiDAR standard elevation metrics extracted with FUSION, the KDE (kernel density estimation) metrics were considered essential to differentiate the layers within the canopy because it calculates the number of peak heights (minimum and maximum values and the range between them) using a Gaussian kernel to construct a probability density function for the peaks in each plot. In addition, the Profile Area, a new metric of FUSION V.4.00, was used, which corresponds to the area under the height percentile profile or curve (Hu et al., 2019). Both metrics are considered important in describing canopy vertical structure, so they were computed from ground to maximum height.

Another set of LiDAR metrics based on the canopy structure (LiDAR canopy metrics) were also calculated from ground to treetop following the methodology developed by Lefsky et al. (1999) and amended by Coops et al. (2007). Using the LiDAR point cloud data, for each circular plot the canopy was divided vertically from the ground to the maximum height into 1 metre intervals, resulting in a series of small cylinders, which were then classified into one of four canopy classes. First each cylinder was classified as empty or filled depending on the absence or presence of LiDAR points. After that, the empty cylinders were divided into “Open gap” if they were situated above the canopy and “Closed gap” if they were below it. In the case of the filled cylinders they were classified as “Euphotic” if they were located in the uppermost 65% of all filled cylinders and “Oligophotic” if below it (Figure 4).

Using this same point cloud cylinders, the Weibull density function was used to describe the Canopy Height Distributions (CHD) in the CVP. Weibull function is commonly applied to characterize foliage distribution for various species due to its flexibility in representing various distribution shapes (Lovell et al., 2003; Coops et al., 2007; Zhang et al., 2017; Melo et al.,2018). The two Weibull coefficients, i.e. scale (α_1) and shape (β_1) were fitted as explained in previous studies using LiDAR data (Lovell et al., 2003;

Coops et al., 2007). Scale provides the position and the distribution of the movement in vertical scaling (the shape of the distribution density curve), while shape explains the capacity to increase or decrease the breadth of the distribution.

Density-based LiDAR metrics were also calculated as the proportion of points above the percentiles (1^{st}, 5^{th}, 10^{th}, 20^{th}, 25^{th}, 30^{th}, 40^{th}, 50^{th}, 60^{th}, 70^{th}, 80^{th}, 90^{th}, 95^{th}, and 99^{th}) as was proposed by Zhang et al. (2017). A summary of the LiDAR metrics with their corresponding descriptions are shown in Table 1.

Table 1. *Description of LiDAR metrics for modelling* LAI_e.

LiDAR metrics	Description
LiDAR Standard Elevation Metrics	
All returns	All returns from ground to maximum height of the LiDAR point cloud.
All returns above height threshold	All returns from height threshold to maximum height of the LiDAR point cloud.
Proportion return above height threshold	All returns from height threshold to maximum height of the LiDAR point cloud, expressed as a percentage.
First returns above height threshold	Only first returns from height threshold to maximum height of the LiDAR point cloud.
Proportion of first returns above height threshold	Only first returns from height threshold to maximum height of the LiDAR point cloud, expressed as a percentage.
Canopy relief ratio	Canopy cover generated by FUSION
Skewness and Kurtosis of heights	The skewness and kurtosis of the heights of first returns with respect to the total.
Percentile Heights	The percentiles of the canopy height distributions (1^{st}, 5^{th}, 10^{th}, 20^{th}, 25^{th}, 30^{th}, 40^{th}, 50^{th}, 60^{th}, 70^{th}, 80^{th}, 90^{th}, 95^{th}, and 99^{th}).
Mean, maximum and minimum height	Mean, maximum and minimum height above ground of all points.
KDE (kernal density estimator)	Number of peak heights with minimum and maximum values
Profile area	Area under the height percentile profile or curve
LiDAR Canopy Metrics	
Return proportion	Proportion of returns in each 1 metre of height of the cylinders from the ground to the maximum height
Mean return proportion	Mean of the proportion of returns considering different ranges of interval, for example from the height threshold to the maximum height.
Density-based metrics	The proportion of points above the percentile heights compared to total number of points
Open and Closed gap zones	Proportion of empty cylinders located above and below the canopy, respectively
Euphotic and Oligophotic zones	Respectively, the proportion of cylinders located within the uppermost percentiles (above 65%) of all filled cylinders and those below the same point in the canopy vertical profile
α1 and β1 parameter of Weibull distribution	The scale parameter, α, and shape parameter, β, of the Weibull density distribution fitted to CHD.

2.4. LIDAR metrics selection and LAI_e models

After extraction of the LiDAR metrics and using the selected radius and height threshold, the LiDAR data must be related to LAI_e. Adding the LiDAR standard elevation metrics to those related to CVP computed from the LiDAR point cloud, generates a large dataset of variables that can be used for model development. To address this issue which is common to this type of study (e.g. Pearse et al., 2017; Zhao and Popescu, 2009), the LiDAR metrics to be used need to be decided prior to model development. To do this in this work, the metrics (Table 1) with low correlations with LAI_e ($r < 0.6$) or highly correlated with other variables were excluded and then the candidate metrics were used in the regression analysis.

Stepwise linear and non-linear allometric modelling were chosen in contrast to non-parametric statistical learning approaches, because with small samples, it is usually wise to use simple methods (Pearse et al., 2016). However, the choice of the model for predicting LAI_e from LiDAR data must be determined by the modeller, and in most cases it is dependent on the number of in-situ LAI_e observations available (Zhao and Popescu, 2009).

As final model selection criteria, the coefficient of determination (R^2) and the root mean square error (*RMSE*) were used. R^2 indicates the proportion of variation explained by the model, while *RMSE*, which uses the same units as the dependent variable, gives an idea of the mean error when using the model.

Also, as validation is important in terms of evaluating the predictive performance of any models developed, the leave-one-out cross-validation was used. It considers the difference between the observed value and the predicted value whereby one piece of data in turn is omitted from the analysis to fit the model and the model is fitted to the remaining n-1 data. The cross-validation of each model was based on the analysis of *RMSE* and R^2 statistics.

2.5. LiDAR-LAI_e Map tool

The selected model was used to develop a tool to generate an automatic map of leaf area index at stand level. The processing of LiDAR data at stand level was programmed in a script, including the generation of a Digital Terrain Model (DTM) and CHM models with a pixel size of 10 m. Moreover, the calculation of all LiDAR metrics mentioned above and the selected LAI_e model were incorporated into the tool (Figure 5). The process starts with the selection of the appropriate LiDAR data and the creation in the area of interest (AOI) followed by the calculation of LiDAR metrics and ends with the generation of different raster maps: mean height (H_m), using the 95th Percentile Height; coverage (*FCC*), using the percentage of first returns and LAI_e raster applying the adjusted model.

Results

The LAI_e field estimates ranged from 1.11 to 2.83 in the LAI_e plots established in the study area. The summary of the results (Table 2) shows how the thinning treatments affected some stand variables of interest, such as basal area, which decreased from 21.10-29.85 m^2 ha^{-1} before the thinning to 4.77-5.84 m^2 ha^{-1} after the thinning treatments.

Table 2. *Summary of forest inventory data measured in the field.*

	Control		Treatment 1			Treatment 2		
	BT/AT2015	AT2019	BT2015	AT2015	AT2019	BT2015	AT2015	AT2019
t (years)	13	16	13	13	16	16	16	19
N (trees ha^{-1})	3338	3169	3756	622	545	3664	439	439
G (m^2 ha^{-1})	13.93	15.48	21.10	4.77	5.41	29.85	5.84	7.04
D_m *(cm)*	7.49	7.98	8.31	10.54	11.85	9.85	12.79	14.09
H_m*(m)*	9.27	10.23	-	12.44	13.32	-	12.91	11.41
V (m^3 ha^{-1})	52.54	66.52	-	19.82	26.58	-	36.87	45.41
Mean LAI_e	-	2.54	-	-	2.12	-	-	1.62

Note: BT: Before Thinning, AT: After Thinning, t: Stand age, N: Stems per hectare, G: Basal area, D_m: mean diameter at breast height per plot, H_m: mean height per plot, V: volume, and Mean LAI_e: mean effective leaf area index by treatment.

The LiDAR standard elevation metrics (Table 3) were extracted considering the same sampling radius of 10 metres as used in the LAI_e plots and a height threshold of 5 m because these were the measurements that provided the best agreement with the LAI_e field measurements.

Table 3. *Summary of LiDAR Standard Elevation metrics used to develop the LAI_e models.*

LiDAR Standard Elevation metrics	Mean	Max	Min	sd
Proportion of first returns above 5 metres	76.78	98.95	50.95	13.91
Canopy relief ratio	0.53	0.69	0.39	0.09
5^{th} Percentile	8.01	9.58	5.83	1.20
10^{th} Percentile	9.21	10.82	6.87	1.16
50^{th} Percentile	13.41	20.15	10.20	2.40
80^{th} Percentile	16.63	22.30	11.49	3.44
90^{th} Percentile	17.99	23.09	12.00	3.89
95^{th} Percentile	18.91	23.93	12.33	4.07
Mean height	13.54	18.12	9.91	2.16
SD Height	3.41	5.43	1.70	1.22
Skewness	-0.18	1.05	-1.65	0.81
Kurtosis	3.25	6.26	1.65	1.39
Maximum height	21.46	26.14	13.83	4.34
Minimum height	5.01	5.06	5.01	0.01
KDE (number of peaks)	2.38	5.00	1.00	1.02
KDE maximum	17.47	24.03	10.00	4.74
KDE minimum	10.20	18.65	5.23	3.37
Profile area	53.41	68.93	39.28	8.23

Referring to the LiDAR canopy metrics (Figure 6), the representation of the proportion of LiDAR points in each cylinder reveals three different canopy layers. They were also identified through the different peak heights which are also seen in the KDE LiDAR metrics (Table 3). The first canopy layer corresponds to the sweet chestnut sprouts, and ranges from 1 to 5 metres, though this varied greatly between plots. For example in plot 1 there is almost no resprouting but in plot 21 almost 30% of the return points correspond to this layer. The second canopy layer ranges from 10 to 17 metres and corresponds to the sweet chestnut layer. This layer was identified because it concurs with the inventory field data (Table 2). Finally, the third canopy layer, ranging from 17 to 20 metres, is the oak which appears in some of the plots. In plots from 15 to 21 and plot number 6, the absence of a peak in the 20 m height reveals absence of oak but the rest of the plots each have a peak, of varying magnitude, at around 20 m, meaning the presence of oak. For example plot 3 has a similar presence of both sweet chestnut and oak as the two peaks have a similar proportion of returns, but plot 1 has more sweet chestnut and plot 13 has more oak.

The spatial distribution of the four canopy classes for sweet chestnut coppice (Figure 7) shows that for plots 1 to 14, except for plot 6, the maximum height reached by the trees is more than 20 m, in contrast to the remaining plots where the maximum height is below 20 m. In general, there were more filled cylinders in Oligophotic zones than in Euphotic zones with percentages ranging, respectively, from 15% to 40% and 9% to 21%. In the case of empty cylinders, the proportion that were Closed gap was smaller (18%–34%) than those that were Open gap (15%–56%).

The Weibull function fitted to the LAI_e plots shows there to be different tendencies in the plots with or without oak (Figure 8). In plots with oak a greater proportion of LiDAR points is acumulatted in the sweet chestnut and oak layers, so the peak of the function tend to be in that part of each plot figure, but in the case of the plots with absence of oak, the resprouting layer in most cases accumulate more LiDAR points in that zone, so the peak of the weibull function tend to be in that part of the figure.

The best linear and non-linear models for estimating LAI_e were selected (eq. 1 and 2 respectively) on the basis of goodness-of-fit statistics. In both equations, all parameters were significant at the 5% level.

$$LAI_e = 3.710 \cdot D05 - 5.322 \cdot D08 \quad (1)$$

$$LAI_e = 98.130 \cdot mean\_5\_maximum\ height^{1.315} \cdot D80^{-0.199} \quad (2)$$

where LAI_e is the effective leaf area index, *D05* and *D80* are the density-based metrics above the 5th and 80th quartiles, respectively, and mean_5_maximum height is the mean return proportion from the height threshold (5 metres) and the maximum height.

The values of the statistics used to compare the models indicate that both models performed reasonably in terms of fitting and cross-validation, although the linear model was slightly better, and also had a better R^2 and lower *RMSE*, so was the one finally selected for the LAI_e calculations (Table 4).

Table 4. Goodness-of-fit statistics and validation for the two models.

	Fitting		*Cross-validation*	
	R^2	*RMSE*	R^2	*RMSE*
Linear model (eq.1)	0.82	0.18	0.79	0.20
Non-Linear model (eq.2)	0.79	0.20	0.61	0.27

Figure 9 shows the outputs for a sweet chestnut forest stand of the map tool developed in this study which uses LiDAR data as input for. The results are consistent with field data, which produced values of LAI_e of between 1.11 to 2.83.

Discussion

Characterizing the vertical profile of forest crowns is critical to support forest management activities and maintaining or improving carbon balance and ecosystem services. As such, this study, using LiDAR technology, a canopy vertical profile is created for sweet chestnut coppice in northern Spain, along with a map tool for characterizing forest stands. In addition, different forest management strategies, in this case thinning at two different intensities, are considered.

The LAI_e field results presented here are a reference for this species in the study area in that they consider different forest management activities (thinning intensities). The values for LAI_e found in this work are similar to those of studies based on deciduous forests comprised of other species, although none of them consider management activities (Cutini et al., 1998; Le Dantec et al., 2000), but they do agree with a previous study of forest management in the study area (Prada et al., 2020).

The plot radius and height threshold used to extract LiDAR data in this study were, respectively, 10 m and 5 m. The selection of the optimal radius and height in the extraction of LiDAR metrics for estimating LAI_e has been investigated in depth as they are key factors, and also impact directly on forest characterization. Morsdorf et al. (2006) found that 15 metres was the optimal radius. However, Riaño et al. (2004) found that the estimation of LAI_e from LiDAR data was best when data were selected using a radius similar to the height of the canopy, which is similar to the results of Solberg et al. (2009) where LiDAR data was taken from a plot with a radius of 0.75 times the tree height. With respect to the height threshold, it is important to take into account that the sweet chestnut considered here sprouts from stump. In previous studies this was not taken into account, so although there are some reviews of optimum height threshold (e.g. Pearse et al., 2017), in this case the height threshold was set as 5 metres because it was more or less the height limit of the resprout layer, as well as being the limit established for the start of the canopy of adult trees (Figure 6). However, to obtain more accurate results it would be necessary to adapt these height thresholds to the type of forest stand involved and thus further subsequent would be necessary.

Previous research has demonstrated the adaptability and appropriacy of LiDAR data in differentiating the different canopy layers throughout the vertical profile of the forest (Lesfksy et al., 1999; Lovell et al., 2003), which is essential for the effective planning of silviculture actions (Mkaouar et al., 2018; Melo et al., 2019). In this study canopy layer differentiation provided valuable information on the proportion of each layer that would otherwise have been very difficult to obtain. For example, the greater maximum heights (Figure 6) in some plots were able to be linked to the presence of oak trees, and the KDE data enabled the differentiaition of a canopy layer for oak between 18 and 24 metres, for sweet chestnut from 10 to 13 metres height and around 5 metres for sweet chestnut resprouting. Clearly, being able to identify such canopy characteristics from LiDAR data requires far less investment, both time and money, than having to collect field data. Another important fact is the ability of the LiDAR data to identify the repsprout layer in sweet chestnut coppice, as can clearly be seen in Figure 6. It represents from 0 to 5 metres, more or less, indicating the suitability of the limit threshold of 5 metres that was chosen as it enables the adult canopy to be distinguished.

Additionally, thinning treatment can be seen to have a direct effect on the resprout layer. In plots 15-21 where there was more intensive thinning (Treatment 2), the proportion of LiDAR points related to the resprout layer accounts for a larger proportion of the LiDAR returns, indicating the presence of foliage, than in plots such as plot 1 (a control plot), where the resprout layer is scarcely discernable. This is a direct consequence of the thinnng treatment, which produces an opening in the canopy layer so the light reaches the resprout layer and the resprouts grow more vigorous. A previous study in the study area with sweet chestnut coppice (Prada et al., 2020) using satellite imagery time-series data detected that the year after a thinning its effect is clearly seen but four years later, similar to the time interval in this study, the canopy recovers to pretreatment coverage levels. The resprout layer obviously contributes to this, and the present study provides useful information on how the canopy layers are distributed within forest stands: although satellite images four years after thinning do not distinguish the effects of the thinning treatment, in this work we clearly see how cover in this layer increases as the intensity of the treatment increases.

The canopy volume distributions in Figure 7 shed some light on the vertical structure of sweet chestnut forest. Again, the importance of the resprout layer is demonstrated by the Closed gap zone which reaches up to 5 metres. Above this point, if canopy volume distribution is related to height (Figures 6 and 7), it can be seen that in the plots with the presence of oak (1-5 and 7-14), the Oligophotic zone occupies a greater volume due to the increased presence of sweet chestnut than in the euphotic zone where oak predominates. However, this pattern changes when there is no oak, and the Oligophotic and Euphotic zones tend to have similar volumes. This is the first element of the characterization of the canopy volume distribution in sweet chestnut forest. Other authors have focused on species such as coniferous forest, broad-leaved forest, mixed forest, hemlock and eucalyptus (Lesfky et al., 1999; Lovell et al., 2003; Zhang et al., 2017) and found different canopy volume distributions depending on the site and species.

The selected LAI_e models use different LiDAR metrics in their formulation than other studies, but result in similar R^2 values (Coops et al., 2007; Jensen et al.,2008; Solberg et al., 2009; Zhang et al., 2017). Rather than using regression analysis in modelling the LAI_e, other authors have employed physically-based models, but the resulting R^2 values are also similar to those found in this study (Heiskanen et al., 2015; Korhonen et al., 2011). Other studies such as Pearse et al. (2017) have explored non-parametric techniques since they have used more plots than in this study. However, the importance of this work relies on the fact that it is the first attempt to relate LAI_e with different thinning intensities in sweet chestnut coppice and data related to this type of management intervention are difficult to obtain because it is not often carried out. Consequently, in the future the model can be improved by adding more field information in order to strengthen the LAI_e models for sweet chestnut coppice in the north of Spain.

Finally, the mapping tool developed in this paper allows spatial information to be generated that is of value in implementing management strategies that improve productivity, ecosystem functions, forest management planning and fuel management. While this tool could be further improved with new models and the inclusion of new variables based on LiDAR metrics, the results provided here indicate that the

statistics derived from the LiDAR data, and the models developed based on them, are suitable for calculating CVP and great potential for its analysis (Lovell et al., 2003).

Conclusion

In this study, the methodology used and developed is of great interest because the characterization of the canopy vertical profile is of enormous benefit in terms of improving forest management planning, ecosystem functioning, structural biodiversity and ecosystem services. In this study the descriptive capacity of a set of LiDAR metrics related to standard elevation and canopy structure was assessed with respect to different thinning treatments.

The LiDAR metrics generated from the point cloud help to understand how the different canopy layers are distributed throughout the canopy of sweet chestnut coppice forest stands. The resprout layer was demonstrated to have a high impact on forest vertical structure. On the basis of the height threshold corresponding to average resprouting height, the LiDAR point cloud data could be used to distinguish resprouting from adult trees in the CVP as well as to indicate the presence of other species (i.e. oak) in some parts of the study area. This is a good example of the valuable information that can be obtained from LiDAR data. Also, a full characterization of the canopy was made from the ground to maximum height which provides not only data on the differentiation of the layers already mentioned but also a completed description of the distribution of the different canopy zones.

The results of the LAI_e models demonstrated its reliability in the study area (Cross-validation: R^2 (0.79) and *RMSE* (0.20)). Using these models, the generation of LAI_e maps for the all the study area was possible, but the tool was designed in a way that other LiDAR variables of interest can also be mapped. As a consequence, this information will help forest managers in decision-making planning, allowing them to consider not only productive options, but also the biodiversity and structural parameters of sweet chestnut forest stands.

Declarations

ACKNOWLEDGEMENTS

The authors wish to thank to the Forest Service (Government of the Principality of Asturias) and CETEMAS support staff (Antolín, Manuel and Ernesto) and to acknowledge the Severo Ochoa Asturian fellowship awarded to MP. Thanks also to Ronnie Lendrum, scientific editor and proofreader, for correcting the English of the manuscript.

AUTHOR CONTRIBUTIONS

Marta Prada: Conceptualization, Software, Methodology, Data curation, Validation, Writing- Original draft preparation Elena Canga: Conceptualization, Methodology, Software, Validation, Formal analysis, Writing - Review & Editing, Supervision Juan Majada: Supervision, Project administration Celia Martínez:

Conceptualization, Supervision, Writing - Review & Editing. All authors provided editorial advice and gave final approval for publication.

FUNDING

This work was financially supported through the Proyecto Estratégico del Castaño of the Dirección General de Infraestructuras Rurales y Montes (Consejería de Medio Rural y Cohesión Territorial, Gobierno Principado de Asturias) and a grant from the Severo Ochoa Asturian fellowship awarded to MP.

CONFLICTS OF INTEREST

The authors declare that they have no known competing financial interests or personal relationships that could have appeared to influence the work reported in this paper.

AVAILABILITY OF DATA AND MATERIALS

Not applicable

ETHICS APPROVAL AND CONSENT TO PARTICIPATE

Not applicable

CONSENT FOR PUBLICATION

Not applicable.

References

1. Bergen K M, Goetz S J, Dubayah R O, Henebry G M, Hunsaker C T, Imhoff M L, Nelson R F, Parker G G, Radeloff V C (2009) Remote sensing of vegetation 3-D structure for biodiversity and habitat: Review and implications for lidar and radar spaceborne missions. J Geophys Res Biogeosciences 114 (G2). https://doi.org/10.1029/2008JG000883.
2. Bréda NJJ (2008). Leaf area index. In: Erik S, Brian F (Eds.), Encyclopedia of Ecology. Academic Press, Oxford, pp. 2148–2154.
3. Ceccherini G, Duveiller G, Grassi G, Lemoine G, Avitabile V, Pilli R, Cescatti A (2020) Abrupt increase in harvested forest area over Europe after 2015. Nat 583: 72-77. https://doi.org/10.1038/s41586-020-2438-y.
4. Chen J M, Black T A (1992) Defining leaf area index for non-flat leaves. Plant Cell Environ 15 (4): 421–429. https://doi.org/10.1111/j.1365-3040.1992.tb00992.x
5. Conedera M, Krebs P, Tinner W, Pradella M, Torriani D (2004) The cultivation of *Castanea sativa* (Mill.) in Europe, from its origin to its diffusion on a continental scale. Veg Hist Archaeobot 13(3): 161-179. https://doi.org/10.1007/s00334-004-0038-7.

6. Coops N C, Hilker T, Wulder M A, St-Onge B, Newnham G, Siggins A, Trofymow J T (2007) Estimating canopy structure of Douglas-fir forest stands from discrete-return LiDAR. Trees 21(3), 295. https://doi.org/10.1007/s00468-006-0119-6.
7. Cutini A, Matteucci G, Mugnozza G S (1998) Estimation of leaf area index with the Li-Cor LAI 2000 in deciduous forests. Forest Ecol Manag 105(1-3): 55-65. https://doi.org/10.1016/S0378-1127(97)00269-7.
8. Fang H, Baret F, Plummer S, Schaepman-Strub G (2019) An overview of global leaf area index (*LAI*): Methods, products, validation, and applications. Rev Geophys 57(3): 739-799. https://doi.org/10.1029/2018RG000608.
9. Hamraz H, Contreras M A, Zhang J (2017) Vertical stratification of forest canopy for segmentation of understory trees within small-footprint airborne LiDAR point clouds. ISPRS J Photogramm 130: 385-392. https://doi.org/10.1016/j.isprsjprs.2017.07.001.
10. Heiskanen J, Korhonen L, Hietanen J, Pellikka P K (2015) Use of airborne lidar for estimating canopy gap fraction and leaf area index of tropical montane forests. Int J Remote Sens 36 (10): 2569-2583. https://doi.org/10.1080/01431161.2015.1041177.
11. Hu T, Ma Q, Su Y, Battles J J, Collins B M, Stephens S L, Kelly M, Guo Q (2019) A simple and integrated approach for fire severity assessment using bi-temporal airborne LiDAR data. Int J Appl Earth Obs Geoinformation 78: 25-38. https://doi.org/10.1016/j.jag.2019.01.007.
12. Jensen J L R, Humes, K S, Vierling L A, Hudak A T (2008) Discrete return lidar-based prediction of leaf area index in two conifer forests. Remote Sens Environ 112: 3947–3957. https://doi.org/10.1016/j.rse.2008.07.001.
13. Jonckheere, I, Fleck, S, Nackaerts, K, Muys, B, Coppin, P, Weiss, M, Baret, F (2004) Review of methods for in situ leaf area index determination: Part I. Theories, sensors and hemispherical photography. Agr Forest Meteorol 121(1-2): 19-35. https://doi.org/10.1016/j.agrformet.2003.08.027.
14. Korhonen, L, Korpela, I, Heiskanen, J, Maltamo, M (2011) Airborne discrete-return LIDAR data in the estimation of vertical canopy cover, angular canopy closure and leaf area index. Remote Sens Environ 115(4): 1065-1080. https://doi.org/10.1016/j.rse.2010.12.011.
15. Le Dantec, V, Dufrêne, E, Saugier, B (2000) Interannual and spatial variation in maximum leaf area index of temperate deciduous stands. Forest Ecol Manag 134 (1-3): 71-81. https://doi.org/10.1016/S0378-1127(99)00246-7.
16. Lefsky, M A, Cohen, W B, Acker, S A, Parker, G G, Spies, T A, Harding, D (1999) Lidar remote sensing of the canopy structure and biophysical properties of Douglas-fir western hemlock forests. Remote Sens Environ 70(3): 339-361. https://doi.org/10.1016/S0034-4257(99)00052-8.
17. Lefsky, M A, Cohen, W B, Parker, G G, Harding, D J (2002) LiDAR remote sensing for ecosystem studies: LiDAR, an emerging remote sensing technology that directly measures the three-dimensional distribution of plant canopies, can accurately estimate vegetation structural attributes and should be of particular interest to forest, landscape, and global ecologists. Biosci 52(1): 19-30. https://doi.org/10.1641/0006-3568.

18. Lim, K, Treitz, P, Wulder, M, St-Onge, B, Flood, M (2003) LiDAR remote sensing of forest structure. Prog Phys Geog 27(1): 88-106. https://doi.org/10.1191/0309133303pp360ra.
19. Lovell, J L, Jupp, D L B, Culvenor, D S, Coops, N C (2003) Using airborne and ground-based ranging LiDAR to measure canopy structure in Australian forests. Can J Remote Sens 29: 607–622. https://doi.org/10.5589/m03-026.
20. Mannetti, M C, Enrico, M, Mario, P, Zanuttini, R, Marco, C (2020) Coppice Woodlands and Chestnut Wood Technology. In The Chestnut Handbook; Crop and Forest Management; Beccaro, G, Alma, A, Bounous, G, Gomes-Laranjo, J (Eds.), CRC Press, Taylor & Francis Group: Oxfordshire, UK, pp. 275–295.
21. Magnussen, S, Nord-Larsen, T, Riis-Nielsen, T (2018) LiDAR supported estimators of wood volume and aboveground biomass from the Danish national forest inventory (2012–2016). Remote Sens Environ 211: 146-153. https://doi.org/10.1016/j.rse.2018.04.015.
22. McGaughey, R J (2020) FUSION/LDV: Software for LIDAR Data Analysis and Visualization. USADA. Forest Service. Pacific Northwest Research Station. 212 pp.
23. Melo, A M, Reis, C R, Martins, B F, Penido, T M A, Rodriguez, L C E, Gorgens, E B (2019) Monitoring the understory in eucalyptus plantations using airborne laser scanning. Sci Agr 78(1). http://dx.doi.org/10.1590/1678-992X-2019-0134
24. Menéndez-Miguélez, M, Canga, E, Barrio-Anta, M, Majada, J, Álvarez-Álvarez, P (2013) A three level system for estimating the biomass of Castanea sativa Mill. coppice stands in north-west Spain. Forest Ecol Manag 291, 417-426. https://doi.org/10.1016/j.foreco.2012.11.040.
25. Menéndez-Miguélez, M, Canga, E, Álvarez-Álvarez, P, Majada, J (2014) Stem taper function for sweet chestnut (*Castanea sativa*) coppice stands in northwest Spain. Ann Forest Sci 71(7): 761-770. https://doi.org/10.1007/s13595-014-0372-6.
26. Mkaouar, A, Kallel, A, Guidara, R, Rabah, Z B (2018) Detection of forest strata volume using LiDAR data. In: 4th International Conference on Advanced Technologies for Signal and Image Processing (ATSIP) (pp. 1-6). IEEE.
27. Morsdorf, F, Kötz, B, Meier, E, Itten, K I, Allgöwer, B (2006) Estimation of *LAI* and fractional cover from small footprint airborne laser scanning data based on gap fraction. Remote Sens Environ 104(1): 50-61. https://doi.org/10.1016/j.rse.2006.04.019.
28. Nelson, R F, Gregoire, T G, Oderwald, R G (1998) The effects of fixed-area plot width on forest canopy height simulation. Forest science 44(3): 438-444.
29. Parker, G.G (1995) Structure and Microclimate of Forest Canopies. In Forest Canopies; Lowman, M.D., Nadkarni, N.M.(Eds.), Academic Press: San Diego, CA, USA, pp. 73–106.
30. Pearse, G D, Morgenroth, J, Watt, M S, Dash, J P (2017) Optimising prediction of forest leaf area index from discrete airborne LiDAR. Remote Sens Environ 200: 220-239. https://doi.org/10.1016/j.rse.2017.08.002.
31. Popescu, S C, Wynne, R H, Nelson, R F (2002) Estimating plot-level tree heights with lidar: local filtering with a canopy-height based variable window size. Comput Electron Agr 37(1-3): 71-95.

https://doi.org/10.1016/S0168-1699(02)00121-7.

32. Prada, M, Cabo, C, Hernández-Clemente, R, Hornero, A, Majada, J, Martínez-Alonso, C (2020) Assessing Canopy Responses to Thinnings for Sweet Chestnut Coppice with Time-Series Vegetation Indices Derived from Landsat-8 and Sentinel-2 Imagery. Remote Sens 12(18), 3068. https://doi.org/10.3390/rs12183068
33. Qu, Y, Shaker, A, Korhonen, L, Silva, C A, Jia, K, Tian, L, Song, J (2020) Direct Estimation of Forest Leaf Area Index based on Spectrally Corrected Airborne LiDAR Pulse Penetration Ratio. Remote Sens 12(2), 217. https://doi.org/10.3390/rs12020217.
34. Riaño, D, Valladares, F, Condés, S, Chuvieco, E (2004) Estimation of leaf area index and covered ground from airborne laser scanner (LiDAR) in two contrasting forests. Agr Forest Meteorol 124(3-4): 269-275. https://doi.org/10.1016/j.agrformet.2004.02.005.
35. Richardson, J J, Moskal, L M, Kim, S H (2009) Modelling approaches to estimate effective leaf area index from aerial discrete-return LIDAR. Agr Forest Meteorol 149: 1152–1160. https://doi.org/10.1016/j.agrformet.2009.02.007.
36. Solberg, S, Næsset, E, Hanssen, K H, Christiansen, E (2006) Mapping defoliation during a severe insect attack on Scots pine using airborne laser scanning. Remote Sens Environ 102(3-4): 364-376. https://doi.org/10.1016/j.rse.2006.03.001.
37. Solberg, S, Brunner, A, Hanssen, K H, Lange, H, Næsset, E, Rautiainen, M, Stenberg, P (2009) Mapping *LAI* in a Norway spruce forest using airborne laser scanning. Remote Sens Environ 113(11): 2317-2327. https://doi.org/10.1016/j.rse.2009.06.010.
38. Solberg, S (2010) Mapping gap fraction, *LAI* and defoliation using various ALS penetration variables. Int J Remote Sens 31(5): 1227-1244. https://doi.org/10.1080/01431160903380672.
39. Van Leeuwen, M, Nieuwenhuis, M (2010) Retrieval of forest structural parameters using LiDAR remote sensing. Eur J Forest Res 129(4): 749-770. https://doi.org/10.1007/s10342-010-0381-4.
40. Weiss, M, Baret, F, Smith, GJ, Jonckheere, I, Coppin, P (2004) Review of methods for in situ leaf area index (*LAI*) determination Part II. Estimation of *LAI*, errors and sampling. Agric For Meteorol 121: 37–53. https://doi.org/10.1016/j.agrformet.2003.08.001.
41. Zhao, K, Popescu, S (2009) LiDAR-based mapping of leaf area index and its use for validating GLOBCARBON satellite *LAI* product in a temperate forest of the southern USA. Remote Sens Environ 113(8): 1628-1645. https://doi.org/10.1016/j.rse.2009.03.006.
42. Zhang, Z, Cao, L, She, G (2017) Estimating forest structural parameters using canopy metrics derived from airborne LiDAR data in subtropical forests. Remote Sens 9(9), 940. https://doi.org/10.3390/rs9090940.

Figures

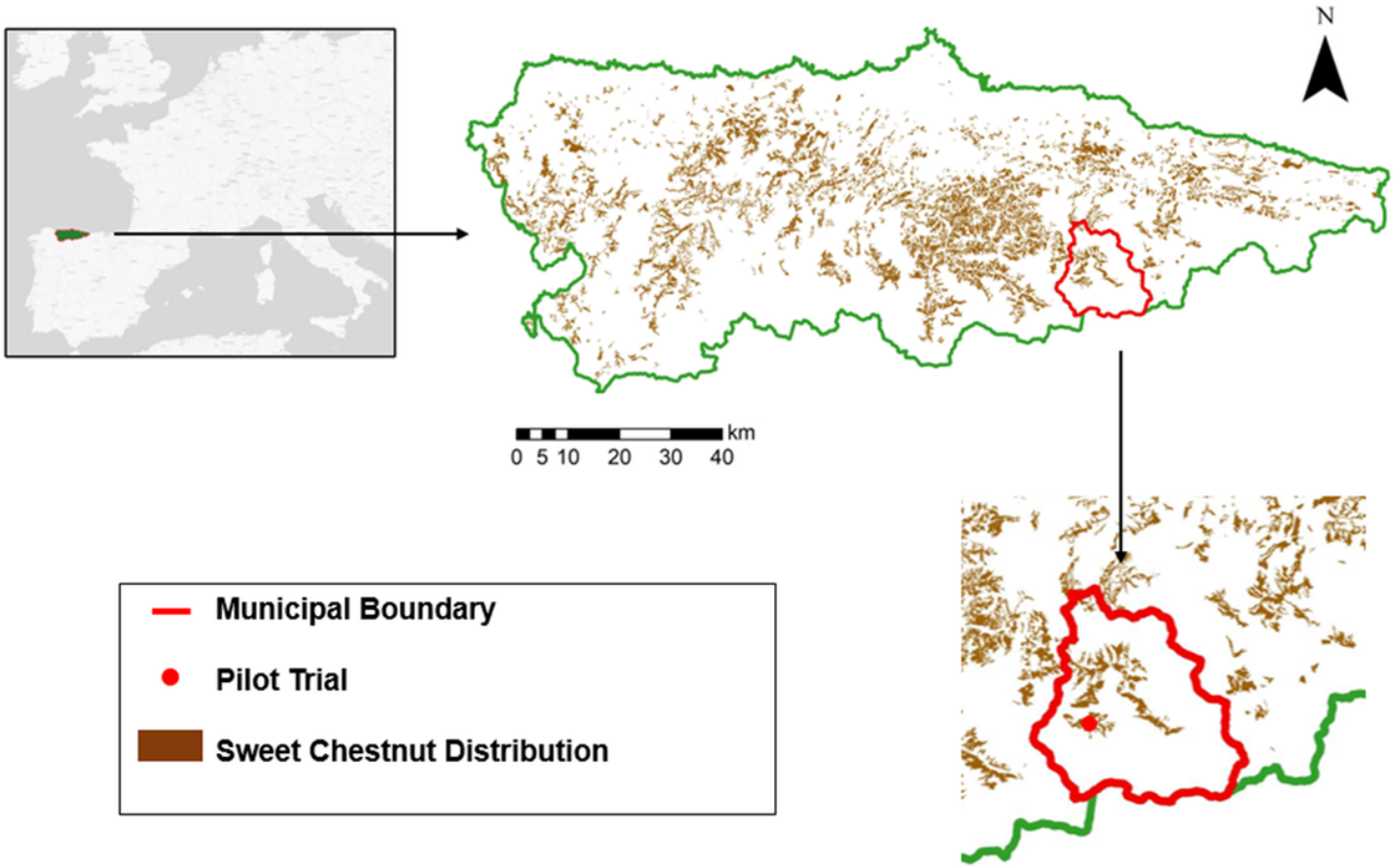

Figure 1

Study area in the north of Spain and location of the forest management pilot trial. Note: The designations employed and the presentation of the material on this map do not imply the expression of any opinion whatsoever on the part of Research Square concerning the legal status of any country, territory, city or area or of its authorities, or concerning the delimitation of its frontiers or boundaries. This map has been provided by the authors.

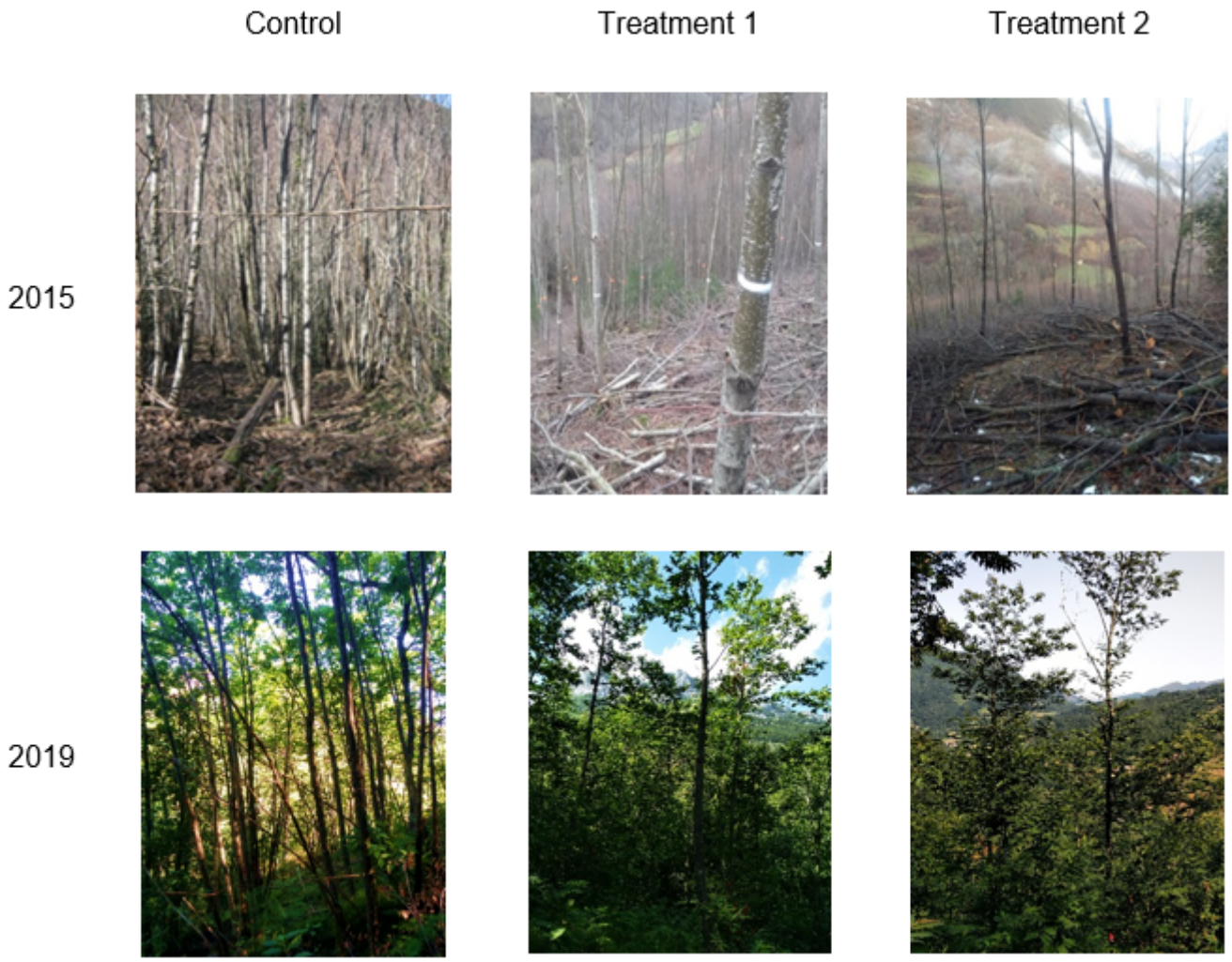

Figure 2

Examples of the Treatments after the thinning in 2015 (installation year) and in 2019.

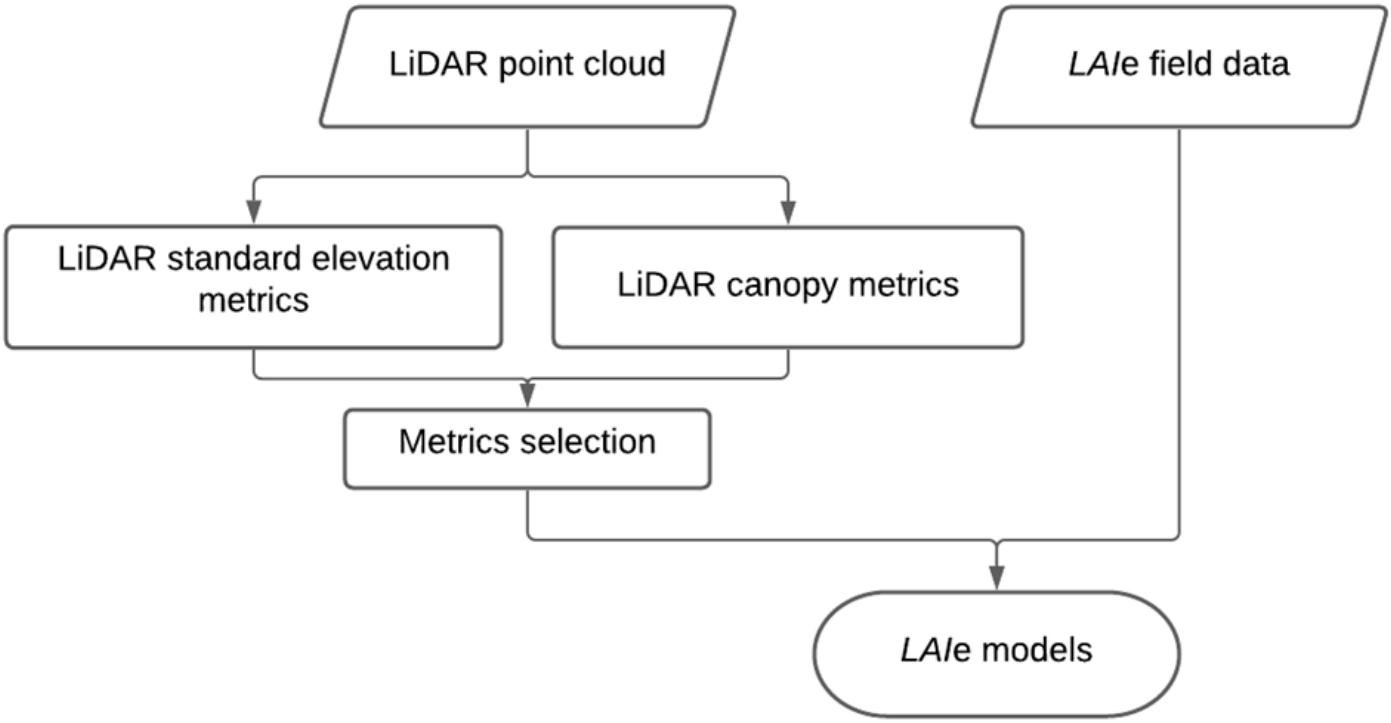

Figure 3

Workflow to obtain LAIe models from LiDAR data.

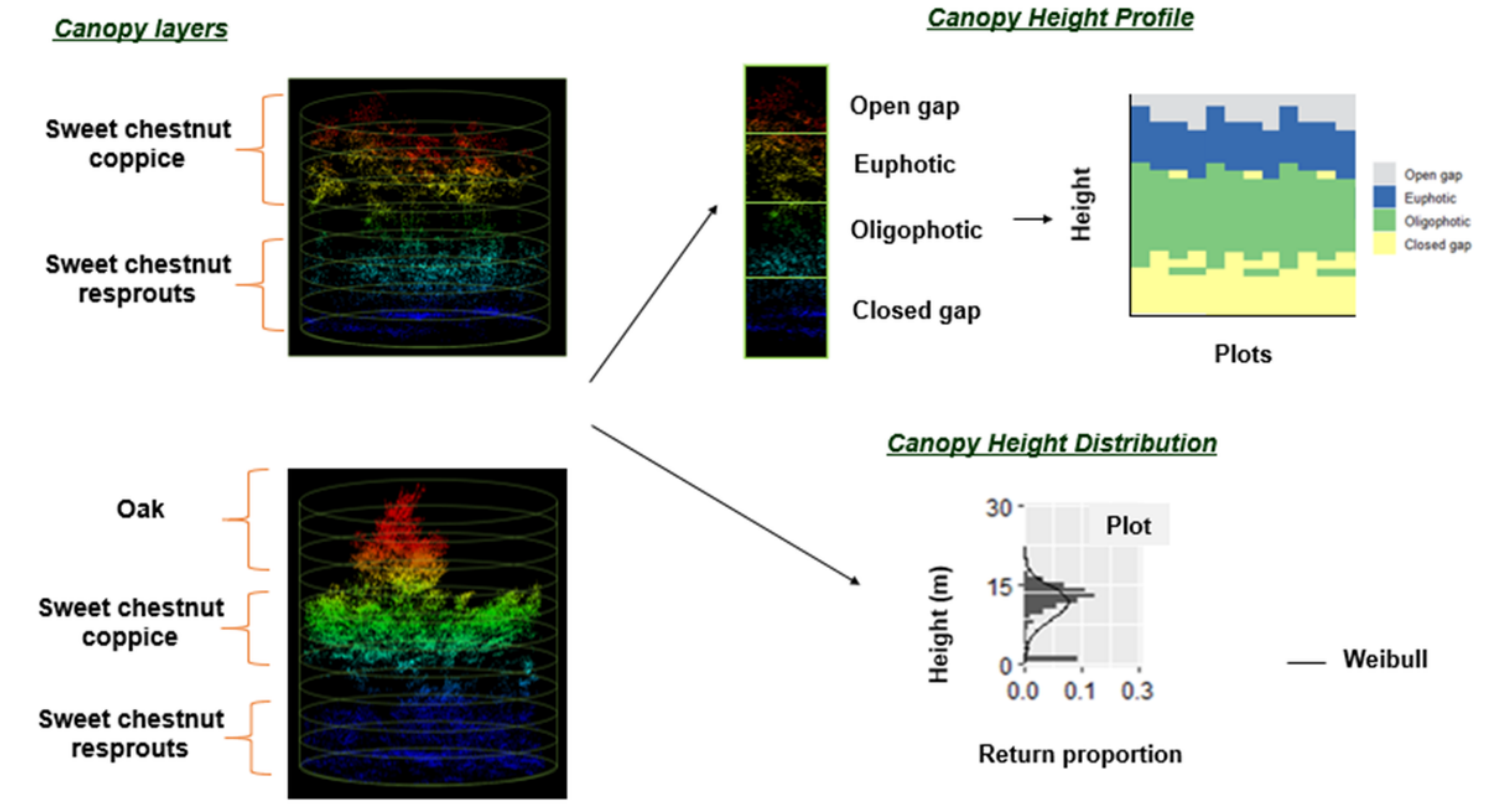

Figure 4

LiDAR metrics based on the canopy structure

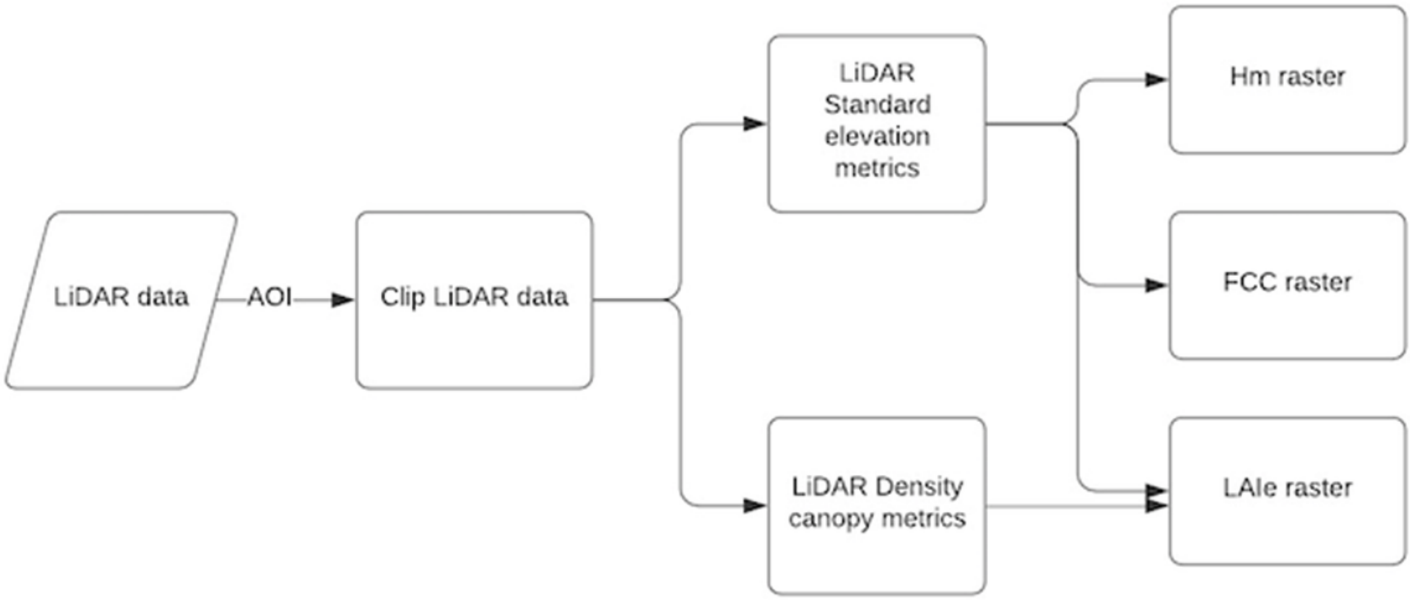

Figure 5

Flowchart of the steps involved in developing the automatic tool for generating the Hm, FCC and LAIe maps

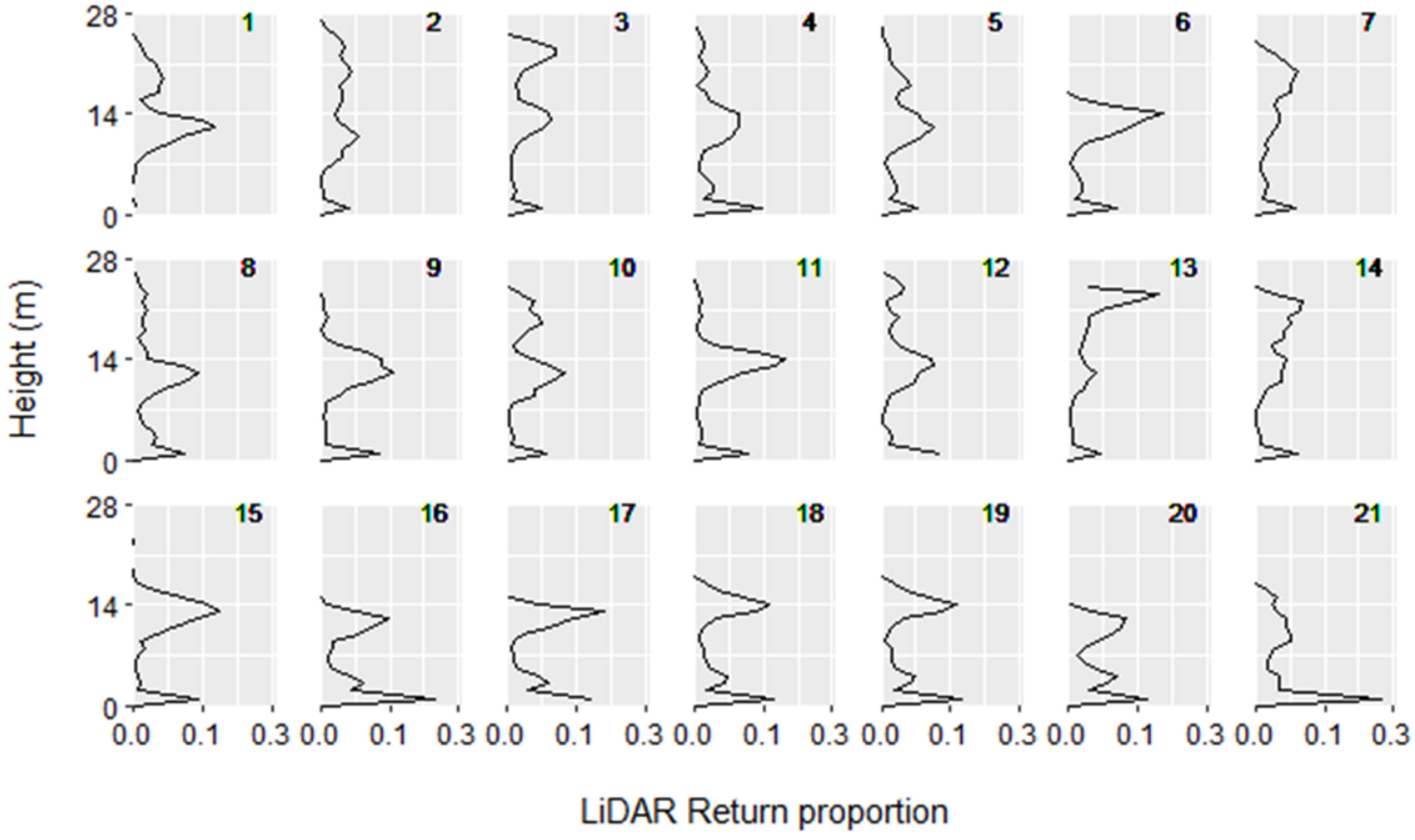

Figure 6

Proportion of LiDAR points in each cylinder in the LAIe plots.

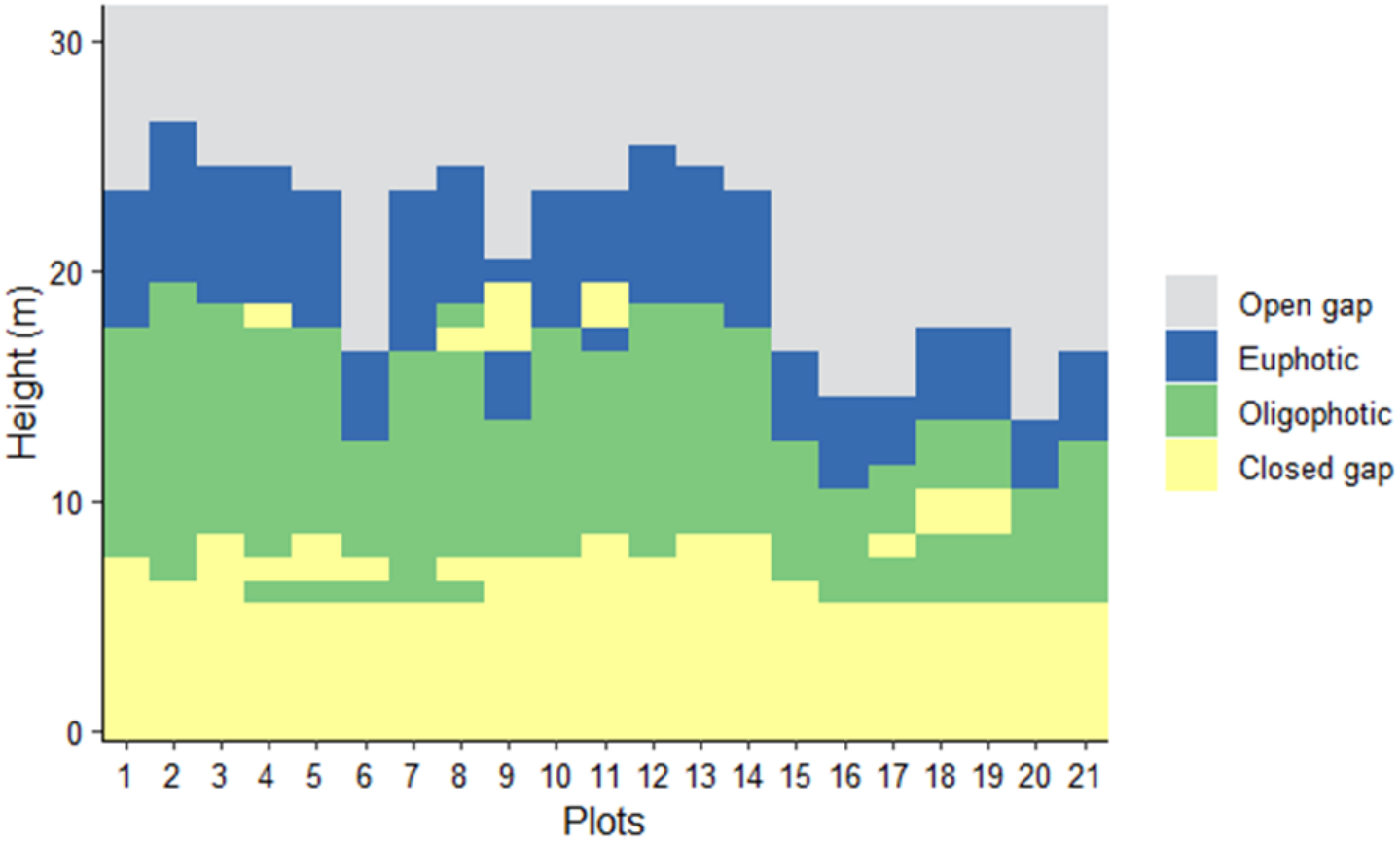

Figure 7

Canopy volume distributions for the plots in sweet chestnut coppice.

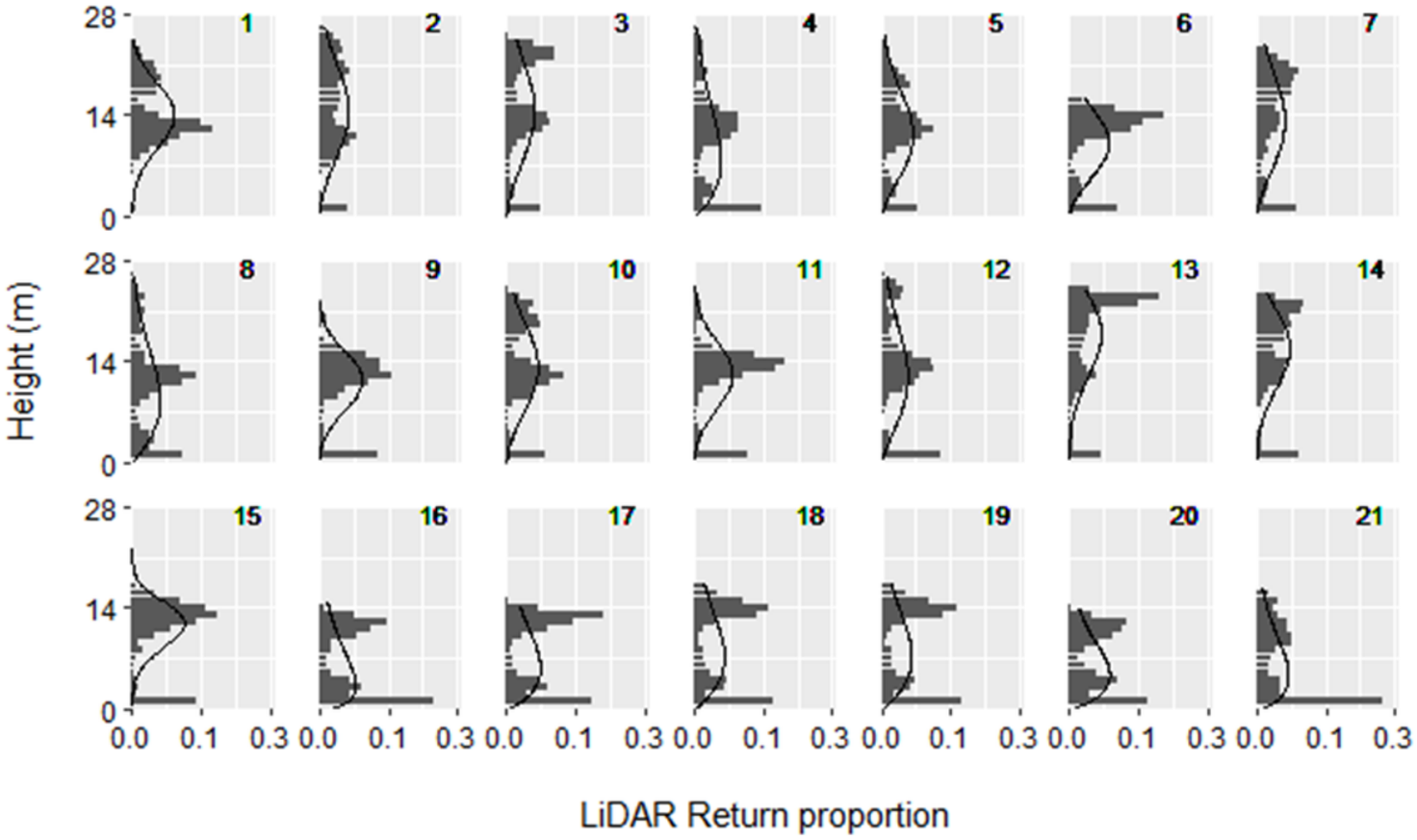

Figure 8

Canopy height distribution by plot. The grey bars represent the LiDAR return proportion for each height interval of 1 metre (from ground to highest point) and the black lines represent the fitted Weibull function for each plot.

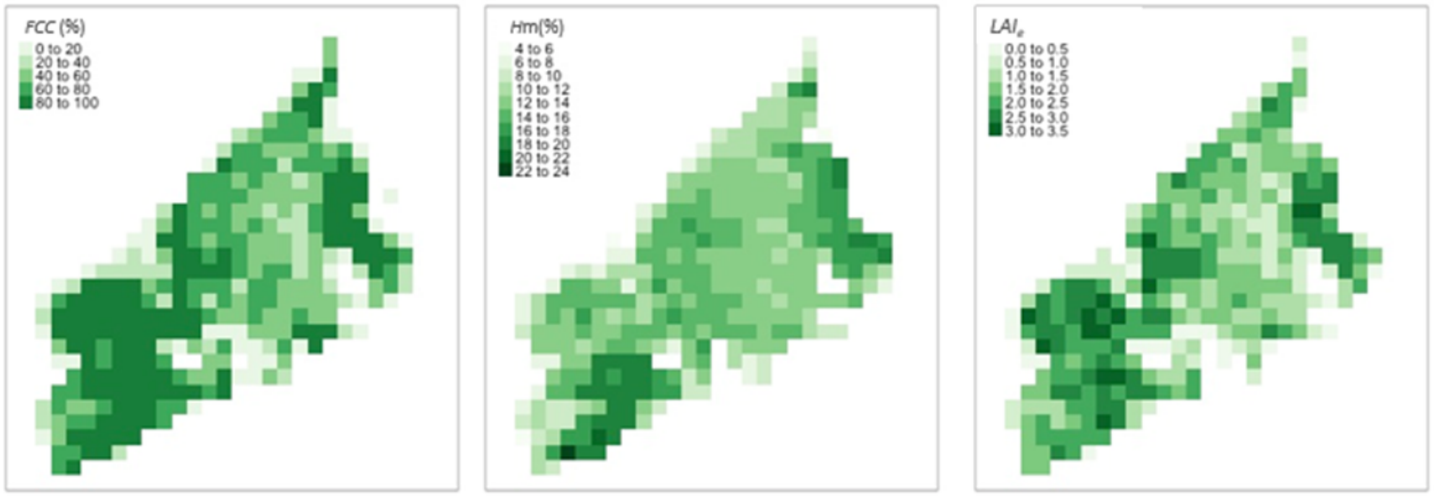

Figure 9

Outputs from the map tool developed in this study: (a) coverage (b) 95th percentile, representing the height of the sweet chestnut forest standard (c) LAIe values obtained using the LAIe model developed in

this study.